Gelatin/Polyethylene glycol/g-C_3N_4 hydrogel with olive oil as a sustainable and biocompatible nanovehicle for targeted delivery of 5-fluorouracil

Milad Rahmani[a], Mehrab Pourmadadi[b], Majid Abdouss [c] , Abbas Rahdar[d], Ana M. Díez-Pascual[e, *]

[a] School of Chemistry, College of Science, University of Tehran, Tehran, Iran
[b] Department of Biotechnology, School of Chemical Engineering, College of Engineering, University of Tehran, Tehran, Iran
[c] Chemistry Department, Amirkabir University of Technology, Tehran, 1591634311, Iran
[d] Department of Physics, Faculty of Sciences, University of Zabol, Zabol 538-98615, Iran, a.rahdar@uoz.ac.ir
[e] Universidad de Alcalá, Facultad de Ciencias, Departamento de Química Analítica, Química Física e Ingeniería Química, Ctra. Madrid-Barcelona, Km. 33.6, 28805, Alcalá de Henares, Madrid, Spain

*Correspondence: am.diez@uah.es (A.M. Díez-Pascual)

Abstract:

5-fluorouracil (5-FU) is an anticancer drug with poor water solubility and stability, leading to short plasma half-time and undesired toxic effects on normal tissues. Therefore, novel drug delivery systems (DDS) are required to improve its therapeutic efficiency. The use of nanoparticles in DDS has emerged as a promising method for controlling the release of chemotherapy drugs. In this study, a novel, sustainable and pH-sensitive nanocomposite was designed for the targeted delivery of 5-fluorouracil (5-FU) against breast cancer cells. The nanodelivery system is based on graphitic carbon nitride (g-C3N4) coated with Gelatin (G)/Polyethylene glycol (PEG) biopolymers, and was prepared by W/O/W double emulsion technique using olive oil and span 80 surfactant. Successful loading of 5-FU into the nanovehicle was confirmed by infrared spectroscopy and X-ray diffraction analyses. Dynamic light scattering corroborated the monodispersity of the nanocarriers, with a typical size between 250 and 300 nm. Scanning electron microscopy images revealed the homogeneity of the nanocomposite and its spherical shape, which was appropriate for DDS. The average zeta potential was +35.4 mV, demonstrating the good stability of the nanocomposite. The drug loading (47%) and encapsulation efficiency (89%) were higher than those reported for other 5-FU nanocarriers. A continuous and controlled 5-FU release from the nanovehicle was observed, and the release rate at pH 5.4 (simulating a cancerous environment) was higher than at pH 7.4 (physiological conditions). Kinetic studies suggested a diffusion controlled mechanism of 5-FU release from the nanocarrier in an acidic environment, while an anomalous transport prevails at neutral pH. The 3-(4,5-dimethylthiazol-2-yl)-2,5-diphenyltetrazolium bromide (MTT) assay revealed that G/PEG/g-C_3N_4 had a significant cytotoxicity on MCF-7 breast cancer cells. Flow cytometry indicated that G/PEG/g-C_3N_4/5-FU led to much higher apoptotic percentage than free 5-FU, while the free drug showed higher percentage of necroptotic cells. This novel bio-nanocomposite shows great potential as a pH-sensitive DDS against breast cancer cells.

Keywords: Bio-based hydrogel; sustainable nanocomposite; drug delivery system; essential oils; gelatin; graphitic-carbon nitride

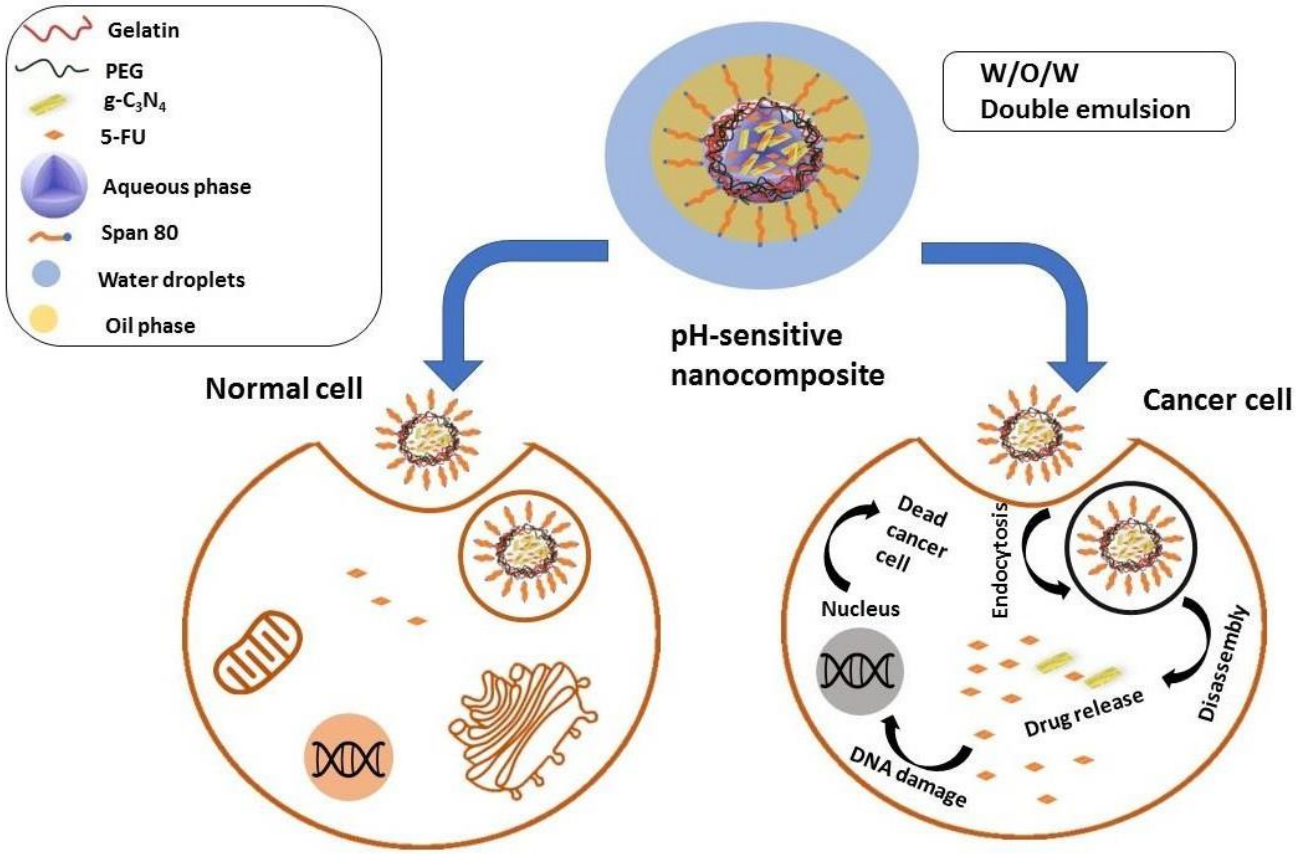

Graphical abstract. Schematic illustration of the release of 5-FU from the bionanocomposite in different mediums.

1. Introduction:

Drug delivery systems (DDS) incorporating nanoparticles are widely used in cancer treatment due to their distinguished features. For instance, they can monitor drug release at the proper dosage and time in the targeted area and remain in the circulatory system for an extended period (Mohebali, 2021). Being nanosized, they easily penetrate the tissue system, thus facilitating drug uptake by the cells and enabling efficient drug delivery at the targeted location. Graphitic carbon nitride (g-C_3N_4) is a novel metal-free biocompatible and biodegradable nanostructure synthesized via heating a carbon and nitrogen-rich precursor that has attracted much attention in biological and biosensing applications (Habibi et al., 2019). This nanomaterial shows specific features, such as large specific surface area, inexpensiveness, sustainability, high thermal and chemical stability, pH-sensitivity and high penetration into body tissues, which are all suitable for cancer treatment (Duan et al., 2018). Zhang and colleagues (Zhang et al., 2013) synthesized g-C_3N_4 nanosheets for

bioimaging applications. An MTT assay with HeLa cell line as the model drug was used to evaluated the biocompatibility and cytotoxicity of the nanosheets. Even at the highest doses (600 μg/mL), no cellular mortality was observed, which demonstrates the high biocompatibility of g-C_3N_4 nanosheets.

5-fluorouracil (5-FU) is a synthetic drug widely used to treat several forms of cancer, like breast, colorectal, and brain (Zhu et al., 2021). It inhibits cell division by affecting DNA synthesis. However, multidrug resistance caused by poor water solubility and stability, long-term use and the nonspecific cytotoxicity have limited the clinical efficacy of this chemotherapy drug (Lee et al., 2016). Therefore, innovative DDS are required to reduce its side-effects, enhance its therapeutic effectiveness and extend its blood circulation time. Previous studies (Yi et al., 2010) demonstrated that 5-FU-loaded PEG-hydrogel is suitable for the development of anticancer DDS, and that the drug-loaded hydrogel was more effective in preventing tumor growth than the free 5-FU.

Hydrogels are 3D chemically cross-linked polymeric networks with hydrophilic groups formed via physical and/or chemical cross-linking methods (Pourmadadi et al., 2023a; Yi et al., 2022). They can be tailored to respond to different environmental conditions, including temperature, pH, and enzymatic activities within pathological sites (Mckenzie et al., 2015). The metabolic activity of cancerous cells results in increased H^+ concentration, leading to a lower pH in tumor tissues compared to healthy ones (Norouzi et al., 2016). Consequently, pH-sensitive hydrogels can be designed using polymers with ionizable chemical groups that can act as proton acceptors or donors, thereby undergoing modifications in response to changes in the pH of the medium. Alternatively, polymeric systems with acid-sensitive bonds can be used, and the cleavage of these bonds facilitates the release of the anchored molecules and drugs at specific anatomical locations with a specific pH within the body or in the area of cancer cells with lower pH (Malekimusavi et al., 2019). Polyethylene glycol (PEG) is a biocompatible water-soluble polymer widely applied in the drug delivery field, due to its long history of safety in humans and classification as Generally Regarded as Safe (GRAS) by the FDA. It is extensively used to coat the surface of therapeutic drugs in order to improve biocompatibility and resist interactions with the components of the blood stream, imparting "stealth" properties (Schöttler et al., 2016). Deng et al. (Deng et al., 2019) synthesized PEG-polycaprolactone (PCL) injectable and heat-sensitive hydrogels for use in drug delivery and tissue engineering, and reported improved properties such as easy drug mixing with the carrier due to their low viscosity at room temperature. PEGylated g-C_3N_4 quantum dots have been used as a novel, nontoxic and pH-sensitive drug carrier to load doxorubicin (Dong et al., 2018b), and a controlled drug release behavior was observed.

Gelatin (G) is a protein obtained by thermal denaturation of collagen, the main constituent of connective tissue. It is one of the most attractive hydrophilic biomacromolecules in biomedical applications including drug delivery systems and tissue adhesives due to its biocompatibility, biodegradability, non-toxicity, low cost, low antigenicity, and ability to stimulate cellular attachment and growth (Houshyari et al., 2018). Given that its phase behavior in solution changes with pH and temperature, it is an excellent material for targeted drug delivery (Ethirajan et al., 2008). For instance, Curcio and coworkers (Curcio et al., 2013) prepared a biocompatible and pH-responsive gelatin-based nanosphere for delivery of diclofenac sodium salt. Drug release profiles

were evaluated at different pHs and a complete drug release was observed in the presence of pancreatin in 30 h. Through cross-linking of G and PEG to form a G/PEG copolymer, the physical strength of the hydrogel and the control of the drug release were notably enhanced.

In this study, a hydrogel comprising G and PEG polymers was prepared, and g-C_3N_4 was chosen as a pH-responsive and non-toxic filler. The main goal was to develop a novel, biocompatible and pH-responsive nanocomposite for sustained and targeted drug delivery. In particular, this design aims to increase the half-life of 5-FU in the bloodstream and reduce its side effects. To the best of our knowledge, G/PEG/g-C_3N_4 biocompatible nanocomposite has not been reported earlier, nor applied as a DDS. 5-FU drug was loaded into the hydrogel nanocomposite by a double emulsion of water-in oil-in-water (W/O/W) method, which significantly expands the drug release time since it is released from the internal to the external phase through an oil layer, which acts as a liquid membrane. This represents a significant scientific advance of relevance to the field of study. Further, this method led to the development of a highly stable and uniform G/PEG/g-C_3N_4 /5-FU nanocomposite with a core-shell structure, comprising the drug-loaded g-C_3N_4 nanosheets as the core covered by the G/PEG copolymer and span 80 surfactant as the shell. The synthesized nanocarrier was comprehensively characterized via a number of techniques to get information about its crystalline structure, surface functional groups, morphology, size, surface charge, drug loading and encapsulation efficiency, drug release kinetics and cytotoxicity.

2. Materials and methods

2.1. Materials

Gelatin (G, $C_6H_{12}O_6$, Mw = 180 g/mol), acetic acid and Span 80 were purchased from Merck (Germany). 5-fluorouracil (5-FU, $C_4H_3N_2FO_2$, M_w = 130.078 g/mol) was obtained from EBEWE Pharma (Austria). Phosphate buffer saline (PBS, pH = 7.4) was provided by Gibco (USA). Melamine and polyethylene glycol (PEG, average Mw = 3000 Da) were supplied by Sigma Aldrich (Germany). Olive oil was obtained from S.D. Fine-Chem (India). Fetal bovine serum (FBS) was supplied by WelGENE (Daegu, Republic of Korea). All the solutions were prepared utilizing double-distilled water.

2.2. Synthesis of g-C3N4

g-C_3N_4 nanosheets were prepared by pyrolyzing melamine, following a procedure similar to that reported earlier (Lin et al., 2014). In short, 10 g of melamine was placed in an alumina crucible with a cover and then heated to 600 °C in a muffle furnace for 2 h, and then gradually lowered to room temperature. The resulting yellow powder was sonicated in distilled water for 6 h and subsequently centrifuged at 12,000 rpm for 20 min. Scheme 1 illustrates the different steps for the g-C_3N_4 preparation.

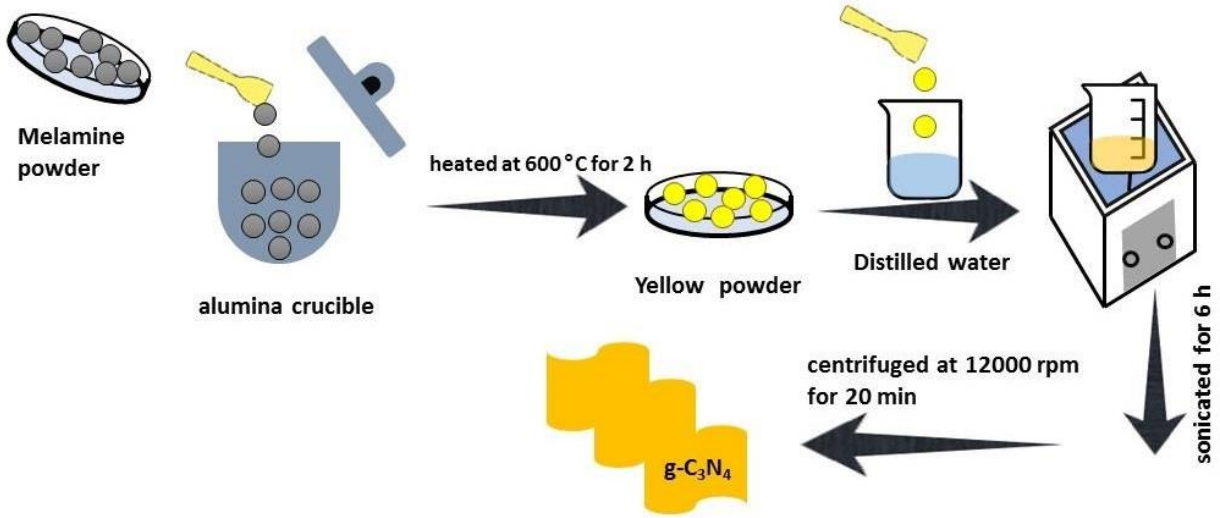

Scheme 1. Schematic representation of the g-C_3N_4 preparation.

2.3. Preparation of G/PEG/ g-C_3N_4 hydrogel nanocomposite and 5-FU loading

Firstly, 2 g of G were added to 100 mL of 2% v/v acetic acid on a stirrer and kept stirring under ambient condition until G had completely dissolved. After that, 0.5 g of PEG powder was added and the mixture was sonicated for 30 min until it was fully dissolved. Afterward, 100 mg of g-C_3N_4 was added to the solution, and the mixture was held under magnetic stirring at 500 rpm until a homogeneous hydrogel was formed. 0.5 mL of the drug solution at a concentration of 1 mg/ml was added dropwise to the G/PEG/g-C_3N_4 hydrogel, and the final concentration of 5-FU within the hydrogel was 5 µg/mL. The mixture was kept, under continuous sonication for 30 min followed by magnetically stirring at 500 rpm for another 30 min until a uniform hydrogel containing 5-FU was obtained with a drug-to-hydrogel ratio of 1:200. The entire drug loading process was carried out at ambient temperature (25 °C) without the need for any specialized equipment.

2.4. Preparation of the double emulsion

20 mL of the homogeneous 5-FU-loaded hydrogel prepared in the former stage was added dropwise with the aid of a syringe to 60 mL of olive oil (hydrophobic phase) mixed with 2% v/v Span 80. The surfactant was used as an emulsifying agent to reduce the surface tension between the oil and aqueous phases thus facilitating the combination of these two phases and increasing emulsion stability. The water-soluble head of the surfactant, acting as the hydrophilic region, interacts with the aqueous phase via hydrogen bonding formation between its OH groups and the water molecules of the solution. Simultaneously, the carbon chain tail, acting as the hydrophobic region, interacts with the oil phase through van der Waals forces (Requena et al., 1977). The oil phase covers the liquid phase and acts as a liquid membrane, regulating the drug release from the internal phase to the external phase (Pourmadadi et al., 2023b). This led to the formation of a spherical water-in-oil primary emulsion comprising the drug in the hydrophobic phase. Subsequently, it was emulsified by addition of an aqueous phase to produce a nano-sized double emulsion. For this purpose, 60 mL of deionized water (hydrophilic phase) was added dropwise and the mixture was then kept for 20 min without agitation in order to separate the 5-FU-loaded

nanocarriers from the hydrophobic phase. Three layers were then formed that were separated due to their different densities: the aqueous layer (bottom, W), the layer containing the hydrogel and the 5-FU-loaded nanosheets (middle, W), and the oil layer (top, O). A sampler was used to separate the oil phase, and the hydrophilic layer was centrifuged at 6,000 rpm for 10 min to separate the nanocomposite from the aqueous phase. The W/O/W method has been proven to be effective in reducing particle size and achieving a hydrogel nanocomposite with uniform dimensions (Eslami et al., 2016). Finally, samples were frozen in a freezer at −20 °C and then pulverized using a freeze dryer to obtain a homogenous powder. Scheme 2 depicts the different stages of the synthesis process.

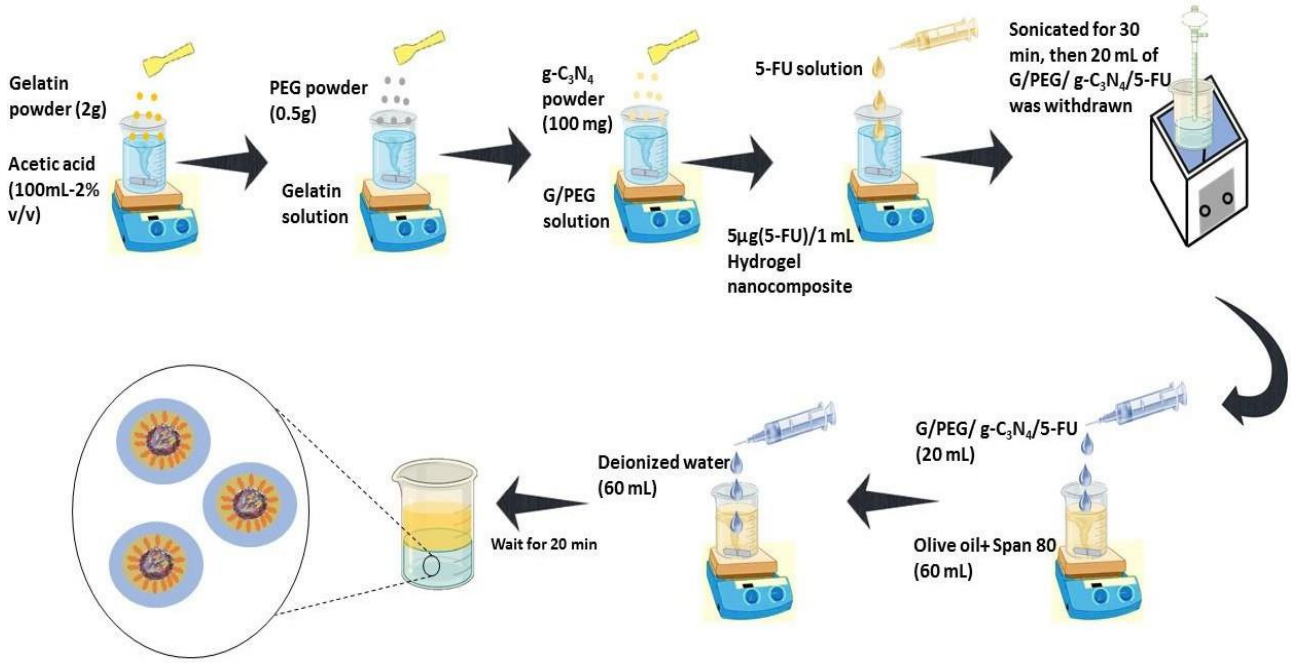

Scheme 2 Schematic representation of the synthesis of G/PEG/g-C_3N_4/5-FU nanocomposite.

2.5. 5-FU loading and encapsulation studies

To get information about the percentage of drug loading (DL) and encapsulation efficiency (EE), the final nanocomposite (1 mg) was mixed with ethyl acetate (1mL). The resulting mixture was stirred in order to dissolve the 5-FU is the ethyl acetate phase. The free 5-FU content in the ethyl acetate phase for each sample was determined via UV-Vis spectrophotomety (Perkin Elmer, lambda 800) at 266 nm, the wavelength at which the drug shows the maximum absorption. The absorbance was calculated using the calibration curve of an aqueous 5-FU solution at 266 nm as reference. The percentages of 5-FU drug DL and EE were calculated using Eqs. 1 and 2:

$$\text{DL (\%)} = \frac{(weight\ of\ loaded\ 5-FU)}{(\text{whole weight of nanoparticle})} \times 100 \quad (1)$$

$$\text{EE (\%)} = \frac{(\text{The whole amount of } 5-\text{FU}) - (\text{unbonded } 5-\text{FU})}{(\text{The whole amount of } 5-\text{FU})} \times 100 \quad (2)$$

2.6. *In-vitro* release study

5-FU has pH-responsive behavior, and the release of 5-FU from G/PEG/g-C_3N_4 was characterized via dialysis process under two different conditions: acetic acid solution at a pH of 5.4 to simulate the acidic tumor microenvironment, and PBS solution at a pH of 7.4 to simulate the normal pH of the blood. The dialysis bags were placed into a beaker at 37°C (normal human body temperature) and stirred constantly with a magnetic stirrer. Subsequently, they were loaded with 1 ml of the G/PEG/g-C_3N_4/5-FU nanocarrier solution. Next, two falcons were provided individually, one containing acidic media and another with the neutral condition, and the dialysis bags were immersed in them. At specific time periods (30 min, 1, 3, 12, 24, 48, 72, and 96 h), 300 µl of each sample was taken out and replaced by the same volume of fresh buffer solution. The percentage of 5-FU released was determined spectrophotometrically using a UV–Vis spectrophotometer (Perkin Elmer, lambda 800) at a wavelength of 226 nm and was calculated according to equation Eq. 3:

$$\text{5-FU released (\%)} = \frac{[5-FU]released}{[5-FU]_{loaded}} \times 100 \quad (3)$$

where *[5-FU] $_{loaded}$* and *[5-FU] $_{released}$* are the amounts of drug loaded into and released from the nanocarrier.

2.7. Culture of cells and cytotoxicity study

The MTT assay was used to assess the cytotoxicity of the different samples, including G, G/PEG, G/PEG/g-C_3N_4, G/PEG/g-C_3N_4/5-FU and free 5-FU on breast cancer cells (MCF-7 cell lines). The control cells were grown in a humidified 37°C/5% CO_2 incubator with high glucose DMEM media supplemented with 10% FBS and 1% penicillin/streptomycin. For this experiment, control cells were seeded at a density of 2×10^4 cells/well into a 96-well microplate and then incubated overnight to allow for the attachment process and to reach a cell confluency of 75%. G, G/PEG, G/PEG/g-C_3N_4, G/PEG/g-C_3N_4/5-FU, and unbonded 5-FU were added to the cells at a concentration of 5 µg/m, followed by another round of incubation for two days. Cells that were not subjected to any treatment were used as a control. 20 µL of the MTT reagent in PBS (pH = 7.4) at a concentration of 5 mg/ml was added to each well and incubated for another 4 h at 37 °C under dark conditions. Then the cell supernatants were separated, and 200 µl of DMSO solution was poured into each well. After agitation for 15 min, the water-insoluble formazan crystals were solubilized by DMSO. The absorbance values of the product were measured at 570 nm using a microplate reader. The percentage of cell viability was estimated according to Eq. 4, where $[A]_S$ is the absorbance of the treated group and $[A]_C$ the absorbance of the control group.

$$\text{Cell viability (\%)} = \frac{[A]_S}{[A]_C} \times 100 \quad (4)$$

2.8. Cell apoptosis analysis

An Annexin *V*-FITC and propidium iodide (PI) double staining kit was used to detect apoptosis and necrosis. A 96-well plate containing about 2×10^4 MCF-7 cells per well was used for the cell culture, and the cancerous cells were left to grow for 24 h before starting the treatment. Cancer cells were treated with G, G/PEG, G/PEG/g-C_3N_4, G/PEG/g-C_3N_4/5-FU, and the free drug at a concentration of 5g/mL and incubated for 48 h. The untreated cells served as control. After 15 minutes of incubation in darkness, cells were removed, washed with PBS, suspended in 100 µL binding buffer, and stained with PI and Annexin V-FITC. Finally, the samples were analyzed using a flow cytometry device (Mindray, China).

3. Results and discussion

3.1. FT-IR analysis

FT-IR analysis is a straightforward method to confirm the composition of a material and get information about the functional groups of the different nanocomposite components. G spectrum (Fig.1) shows intense peaks at 3420, 2927, 1635, 1535, 1240, 1072, and 1038 cm^{-1} that can be attributed to O-H and N-H stretching, the C-H stretching of the carbon backbone, C-N stretching of amide I, N-H stretching, C-N stretching of amide III, C-O stretching, and O-H bending, respectively (Kačuráková & Wilson, 2001). On the other hand, the spectrum of PEG reveals peaks at 3428, 2883 and 1468 cm^{-1} and in the region from 1145 to 554 cm^{-1} associated to the O-H stretching, C-H stretching, C-H bending, and the vibration modes of C-O and C-C (Shameli et al., 2012; Sweah et al., 2016). Furthermore, three peaks can be observed in the spectrum of g-C_3N_4 at 1324, 1418, and 1465 cm^{-1} that belong to C-N stretching vibrations of the CN aromatic repeating unit; also the C=N stretching leads to two peaks at 1571 and 1639 cm^{-1} (He et al., 2018; Martha et al., 2013). The characteristic out of plane vibrations of triazine/s-triazine aromatic repeating units was confirmed by the absorption peaks observed at 885 and 807 cm^{-1} (Niu et al., 2012)

A broad peak can be observed in the spectrum of G/PEG at about 3400 cm^{-1}, including hydroxyl groups of PEG and N–H groups of G. Since the aliphatic C-H stretching of G and PEG overlapped, the peak intensity at 2887 cm^{-1} is increased compared with that of pure G. Furthermore, the peak at 1535 cm^{-1} corresponding to C-N bending vibrations cannot be observed, probably due to the interaction between the OH groups in PEG with the NH_2 groups in G. Additional, the amide C=O stretching in G appears as a peak at 1636 cm^{-1}. The vibration modes of C-O shifted to 1148 cm^{-1}, corroborating the incorporation of PEG into the G network (Chieng et al., 2014). G/PEG and G/PEG/g-C_3N_4 nanocomposite exhibit roughly similar absorption peaks, indicating that no new bonds were formed compared with G/PEG nor strong chemical interactions took place; also, the intensity of the peak at 842 cm^{-1} increased, likely because the triazine vibrations in g-C_3N_4 and the C-C and C-O vibrations in PEG overlapped. Moreover, the peak at 1652 cm^{-1} was found to be stronger than expected owing to the stretching of the aromatic C–N rings. Therefore, it is proved that g-C_3N_4 is present in the nanocomposite (Qi et al., 2020). Regarding the spectra of G/PEG/g-C_3N_4/5-FU, an extra peak can be observed at 1735 cm^{-1}, likely due to the C=O stretching of 5-FU. The N-H stretching of 5-FU also causes a broadening of the peak at 3445 cm^{-1}, and a

downshift from 3506 cm^{-1} to 3445 cm^{-1}. These findings demonstrate the successful encapsulation of 5-FU into the nanocomposite.

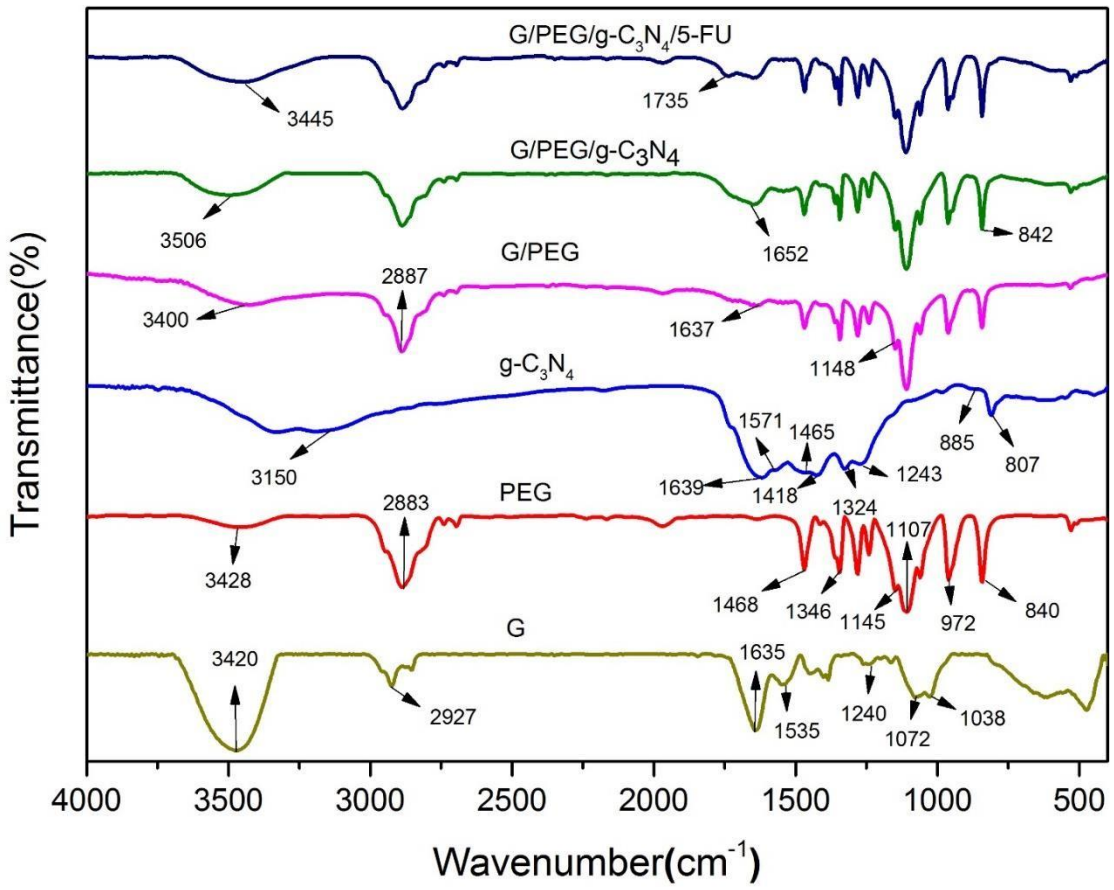

Fig 1. FTIR spectra of G, PEG, g-C_3N_4, G/PEG, G/PEG/ g-C_3N_4, G/PEG/ g-C_3N_4/5-FU.

3.2. XRD characterization

To learn more about the nanocarrier structure and the crystalline nature of its different constituents, the XRD patterns were recorded in a 2θ range of 10-80° and are displayed in Fig. 2. The broad peak at around 2θ = 20° in pure G indicates its amorphous character (Radev et al., 2009). Peaks at 11.3° and 27.8° in g-C_3N_4 are in good agreement with those previously reported for g-C_3N_4 nanomaterials (Liu et al., 2020). The peak at 2θ = 27.8° is ascribed to the (002) plane of the interlayer stacking of graphite-like conjugated aromatic systems, in agreement with the diffraction standard (JCPDS) 87–1526 of g-C_3N_4 nanosheets. Moreover, the low intense peak at 11.3°, assigned to the (100) plane, conforms well to the layered packing structure of tri-s-triazine units (Kumar et al., 2016). The diffractogram of PEG shows peaks at 2θ values of 19.25° (120), 23.3° (032), 27.0° (024), 36.3° (111) and 43° (200), related to the indicated crystalline planes, as reported earlier (Fu et al., 2020). The X-ray diffractogram of G/PEG reveals a considerable reduction in the intensity of the peaks of PEG at 19.25° and 23.3°. This demonstrates the high miscibility and

complexation of PEG with amorphous G. On the other hand, the pattern of G/PEG/g-C_3N_4 displays changes in the intensity of the peaks at around 19° and 23° after adding g-C_3N_4 to the G/PEG hydrogel, corroborating the successful incorporation of g-C_3N_4 into the hydrogel. Furthermore, the characteristic peak of g-C_3N_4 appeared in the diffractogram of G/PEG/g-C_3N_4 at approximately 28°, corroborating the presence of the nanosheets. Further, when 5-FU is added to the hydrogel, π-π stacking and H-bonding interactions with the g-C_3N_4 nanosheets take place (Mahmud et al., 2022). The XRD pattern of G/PEG/g-C_3N_4/5-FU reveals the absence of crystalline peaks of 5-FU as a consequence of its entrapment within the nanocomposite. Moreover, upon drug loading, the characteristic peak of g-C_3N_4 at around 28° decreased significantly, yet another confirmation of the successful entrapment of 5-FU within the g-C_3N_4 nanosheets via H-bonding and π-π stacking forces (Mahmud et al., 2022). Overall, the crystalline structure of G/PEG/g-C_3N_4 became amorphous due to the inclusion of the drug. Therefore, it can be concluded that 5-FU was successfully incorporated into the nanocarrier.

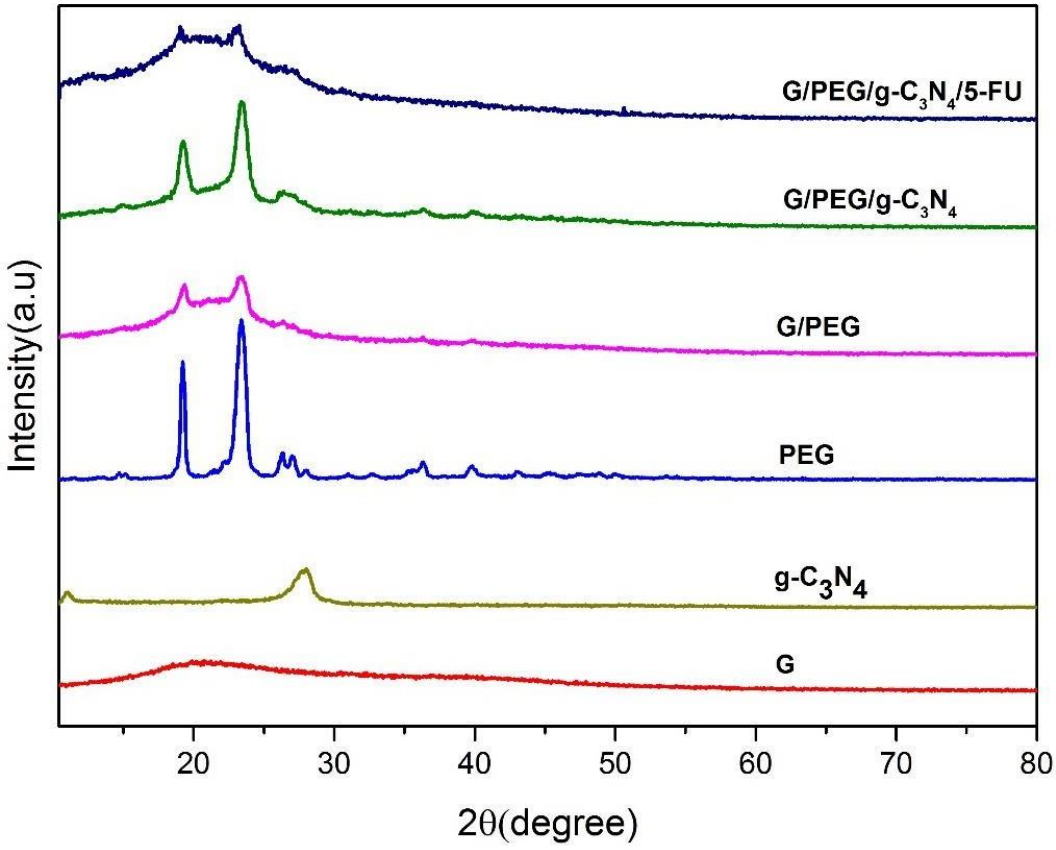

Fig 2. XRD patterns of G, g-C_3N_4, PEG, G/PEG, G/PEG/g-C_3N_4 and G/PEG/g-C_3N_4/5-FU.

3.3. Morphology Study

FESEM images (Fig.3 a,b) showed the morphological characteristics of G/PEG/g-C_3N_4/5-FU. The micrographs reveal that the loaded nanocarrier has a dense structure and is quasi-spherical, with a mean diameter of 270 nm. The spherical form has been reported to be advantageous for DDS. Since the nanocomposite was prepared via W/O/W method, it has a core-shell structure, which is

beneficial for drug delivery applications due to properties such as reduced cytotoxicity, increased dispersibility, more biocompatibility, improved conjugation, and enhanced stability. The core contains the 5-FU-loaded g-C3N4 nanosheets, and the shell comprises the G/PEG copolymer and Span-80 surfactant. The shell is compact with few pores, attributed to the network structure formed by the cross-linking of G and PEG molecular chains. Physical crosslinking can be achieved via hydrogen bonding between the hydroxyl groups of PEG and the amino and ketone groups of G. The shell layer decreases the toxicity of drugs and nanoparticles within the core, enhancing their biocompatibility. Besides, the shell layer can add desirable features like stimuli-responsive behavior to the nanocomposite (Chatterjee et al., 2014). Therefore, the use of W/O/W procedure can enhance drug solubility, which increases bioavailability, and by encapsulating the drug into a nanocomposite, the drug retention in the circulatory system would be increased, which leads to a controlled drug release behavior and a more efficient chemotherapy process.

Dynamic light scattering (DLS) analysis was utilized to examine the size distribution of the nanocomposites. The typical size of G/PEG/g-C_3N_4/5-FU was between 250 and 300 nm (Fig.3 c), with a mean hydrodynamic diameter of 270 nm, in very good agreement with that obtained from FESEM. The polydispersity index (PDI) was found to be 0.36. PDI values lower than 0.5 are indicative of a monodisperse system (Zhao et al., 2013). Moreover, the low PDI obtained is indicative of the uniform size of the nanoparticles. The narrow size distribution and single peak observed hint that the developed nanocarriers are suitable as DDSs.

The zeta potential of G/PEG/g-C3N4/5-FU was +35.4 mV (Fig.3 d). DDS with a zeta potential higher than +30 or − 30 mV are regarded as stable. The strong external repulsion forces among nanoparticles via flocculation or coagulation prevent their aggregation and enhance electrostatic stability. This implies an extended circulation time in the bloodstream and enhances the overall performance of the designed DDS due to an enhanced stability. Regarding the positive overall charge, it should be noted that 5-FU is a weak acid with a pK_a of 7.93 (Zhang et al., 2021). This means that 5-FU is, to a great extent, deprotonated at physiological and intracellular pH. The positive charge of the nanocomposite could be attributed to the amino groups of the G structure, and this corroborates proper polymeric coating. It could also be ascribed to the head group of Span 80 surfactant and olive oil, in agreement with the results of previous works (Prabha and Raj. 2016). This positive surface charge of the nanocarrier would enhance selective cellular uptake and anticancer efficacy (Azizi et al., 2018).

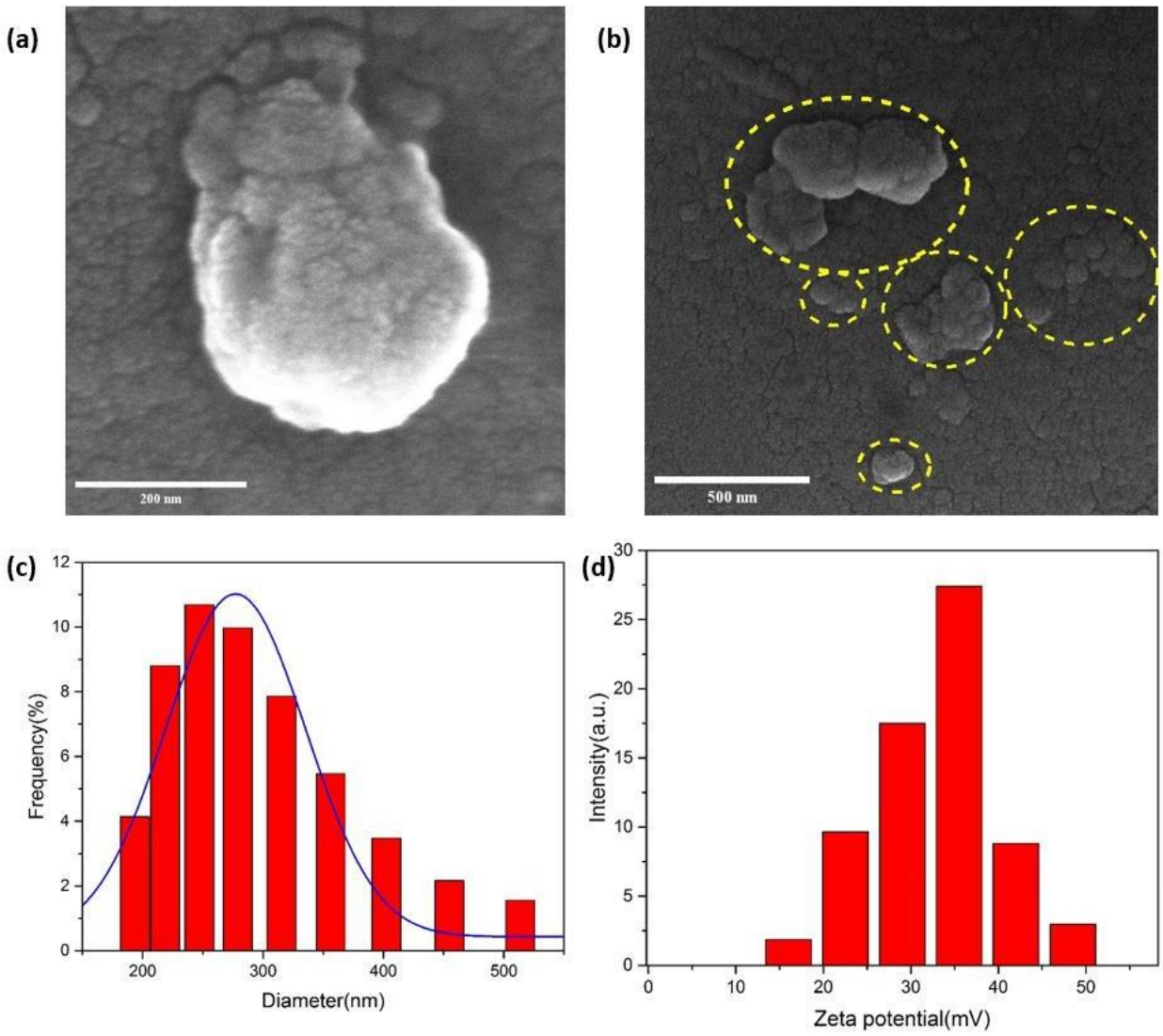

Fig.3 a,b) FESEM images of G/PEG/g-C_3N_4/5-FU at different magnifications. c) Particle size distribution of G/PEG/g-C_3N_4/5-FU obtained from DLS. d) Zeta potential distribution of G/PEG/g-C_3N_4/5-FU.

3.4. Encapsulation and load of drug

Drug loading efficiency (DL) is a crucial factor to compare among DDSs. Achieving high DL is essential for minimizing drug waste and maximizing the nanocarrier effectiveness. Besides, entrapment efficiency (EE) measurement must be precise to prevent overdosing. Researches indicate that the porous structure of the nanoparticles leads to a high drug loading percentage, enabling the entrapment of a high number of drug molecules within themselves. In this study, the drug concentration was determined by UV–Vis spectroscopy at 266 nm after the free drugs were separated from the nanocarriers by dialysis. Using the calibration curve and Eq.1 and Eq.2, EE and DL values of 89% and 47% were calculated, respectively. These parameters play a crucial role on the efficacy of the DDS since they influence the toxicity of the therapeutic system and reduce the wastage of bulk drug substances (Pourmadadi et al., 2023b). The percentages of DL and EE

obtained in this work are higher than those reported previously for other nanocarriers (Table 1). Thus, for co-irradiation-induced cancer therapy, Guo and coworkers (Guo et al., 2020) developed chitosan(CS)-carbon nanocage hybrid-5-FU to attain prolonged drug release, reaching a loading efficiency of about 22.4%; besides, the nanoparticle hybrids were able to trigger cell apoptosis. In another work (Antonio et al., 2017) 5-FU was loaded in CS and CS-carboxy-modified polylactic acid (CS-SPLA) nanocomplexes. Approximately 75% of EE was attained for CS, whereas CS-SPLA revealed an additional 10% increase in EE.

Also, the porous and large surface area of g-C_3N_4 has an important role in attaining such high values because these features allow loading a high amount of 5-FU on the surface. π-π interactions and H-bonding will contribute to the adsorption of 5-FU. The π electrons of C=C and the unshared electron pair of amino groups in the structure of 5-FU can be strongly conjugated with the π electrons of g-C_3N_4 surface (Miralinaghi et al., 2019; Raziq et al., 2017). In addition, H-bonding among functional groups (amino and carboxyl groups) of 5-FU and g-C_3N_4 (primary and secondary amine) is possible, as well as H-bonding among G (amide and hydroxyl groups), PEG (hydroxyl groups), and g-C_3N_4 (CNH_2 and C_2NH). This leads to the formation of a highly interpenetrated biopolymeric network and results in improved entrapment efficiency (Khan et al., 2016; Shameli et al., 2012; Wen et al., 2017).

Table 1 Summary of the drug Loading Efficiency and Encapsulation Efficiency reported for different delivery systems.

5-FU loaded nanocarrier	Loading%	Encapsulation%	Ref.
GO/HPC/CS	3.91	89.24	(Sang et al., 2022)
PLGA-DEX NPs	0.87	65	(Ribeiro et al., 2021)
P(NIPAM-co-AA-co-HEMA)	32.6	57.3	(Zhang et al., 2021)
CS/DEX/CS NPs	------	66.3	(Wang et al., 2020)
CaMg-rGO-40	------	73	(Boddu et al., 2021)
G/PEG/g-C_3N_4	47	89	

3.5. Release results

Due to the high rate of glycolysis in cancer cells, the pH in the extracellular environment of solid tumors is usually lower than that in normal tissues. Therefore, pH-sensitive hydrogels can be designed based on polymers with ionizable chemical groups that can accept or donate protons and undergo modifications in response to changes in the pH of the medium. (Norouzi et al., 2016). The methodology to investigate the different patterns of drug release at two different pHs was described in the materials and methods section. Compared with the normal blood pH (7.4), the pH of the tumor environment is often 5.4. As shown in Fig.4, both pH conditions exhibited an initial rapid release of 5-FU which can be attributed to a small amount of 5-FU physically adsorbed on the surface of the nanocarrier. After that, a slow drug release was observed. At pH 5.4, the release rate shows two stages with a faster release rate, at 3 and 24 h, and then remains almost constant. Conversely, at pH=7.4, the release rate was slowed down at 3 h and then continued almost unchanged. After 24 h, 56% of 5-FU was released at an acid pH, whereas at neutral pH, the nanocarrier was able to retain 72% of the drug. At pH=5.4, 72% of 5-FU was released after 48 h,

while at neutral pH, around 50% of the drug was still encapsulated. Nearly all the 5-FU was released at both pHs after 96 h. Overall, 5-FU release at pH 5.4 was considerably higher than at pH 7.4, corroborating the pH-responsiveness of G/PEG/g-C_3N_4/5-FU. This implies a more efficient release of 5-FU in the tumor environment compared to physiological pH condition, thus reducing drug side effects. Additionally, the kinetic studies in section 3.6 show that the K parameter increased as the pH decreased, yet another confirmation of the faster drug release rate in the acidic environment. Malekimusavi and coworkers (Malekimusavi et al., 2019) explored the release behavior of 5-FU from graphene oxide-L-arginine hydrogel, and found that the drug was released faster under pathological (cancerous) conditions than normal physiological conditions, which is in agreement with the results of the current work. This behavior could be attributed to various factors, such as the pH-responsive nature of g-C_3N_4 nanosheets. At acid pH, the majority of the amine groups of G are protonated and form hydrogen bonds with water molecules due to the pKa of its main aminoacids (9.6, 10.6 and 10.6 for glycine, proline and hydroxyproline, respectively). This protonation leads to an increase in the electrostatic repulsion forces with the hydroxyl groups of PEG, and subsequently, the total free volume of the polymeric network increases. Thus, the matrix expands and this swelling speeds up the drug release in a tumor tissue. Conversely, the polymeric chains are partly deprotonated and more compact at pH = 7.4, and the drug release is gradual. Indeed, the G/PEG copolymer acts as a nanoscale valve. This release pattern is advantageous for DDS since the pH-responsive G/PEG membrane regulates the rate of 5-FU release from porous g-C_3N_4 nanosheets. At neutral pH, the outer polymeric layer prevents drug delivery in normal cells and reduces toxicity to healthy tissues. Thus, this targeting mechanism allows for easier dissolution and more significant release of 5-FU under acidic conditions (Habibi et al., 2019), minimizing its damaging effects on non-cancer cells.

Yi and coworkers (Yi et al., 2010) fabricated a 5-FU-loaded PEG-hydrogel to assess the drug retention time and its anticancer effect. The pharmacodynamic study showed that A549 tumor growth was significantly inhibited in the 5-FU-loaded PEG group compared to the untreated group. Moreover, the drug-loaded hydrogel showed much faster tumor inhibition rate compared to the free drug. In another work, Sun and coworkers (Sun et al., 2013) designed a 5-FU-HAGS (hemostatic absorbable gelatin loaded with 5-fluorouracil) with controlled drug release, demonstrating their suitability for local tumor treatment. The survival ratio of tumor-bearing mice using a 5-FU-HAGS subcutaneous implant was higher than that of mice treated with a subcutaneous injection of 5-FU solution. These examples show the potential of the polymers and drug used in the nanocomposite developed herein for *in-vivo* studies.

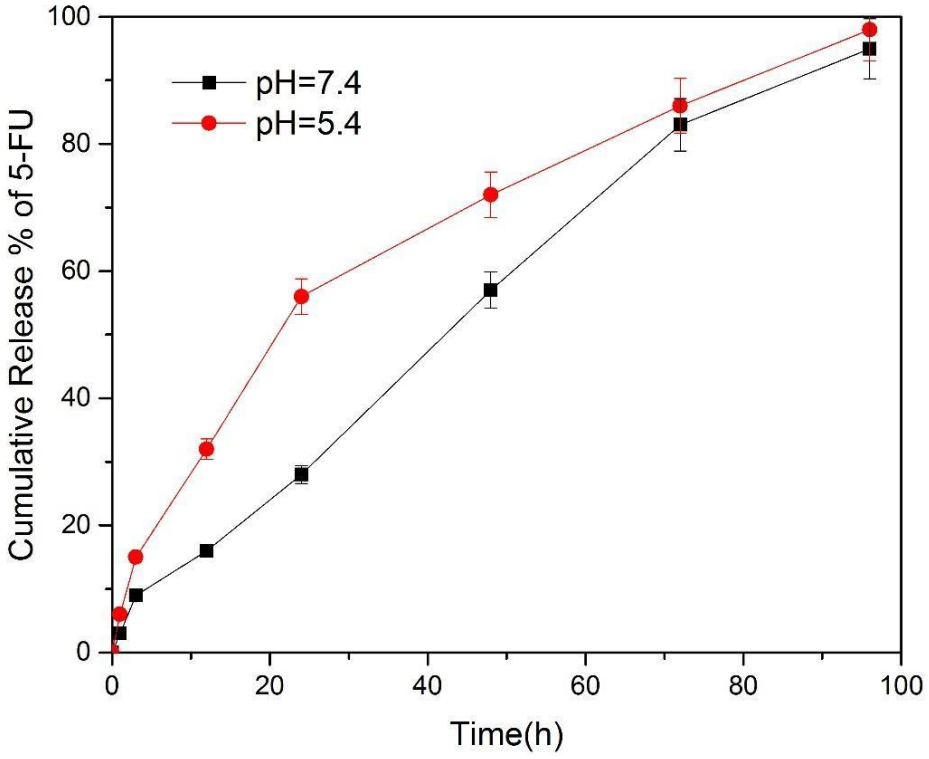

Fig.4 5-FU release profile from G/PEG/g-C_3N_4/5-FU at pH 5.4 and 7.4.

3.6. 5-FU release kinetics

To obtain more information about the release mechanism of 5-FU, experimental data were fitted to four different kinetic models at both pH conditions, as indicated below. Eqs 5, 6, 7 and 8 show the related formula, where Q_t, Q_0, and k (k_0, k_1, k_H, k_{KP}) are the initial amount of the drug in the nanocarrier, the amount of the drug released at time t, and kinetic constant, respectively.

Zero-Order model: $Q_t = Q_0 + k_0 t$ (5)

First-Order model: $\ln Q_t = \ln Q_0 + k_1 t$ (6)

Higuchi model: $Q_t = k_H \sqrt{t}$ (7)

Korsmeyer-Peppas model: $Q_t/Q_\infty = k_{KP} . t^n$ (8)

The model with the highest correlation coefficient (R^2) was chosen as the best-fitting one. The obtained R^2 values and the kinetic constants are collected in Table 2. Clearly, Higuchi model has the highest R^2 (0.992) in an acidic environment. This suggests a diffusion controlled mechanism of 5-FU release from the nanocarrier (Bhasarkar and Bal, 2019). On the other hand, the Korsemyer-Peppas model shows the highest R^2 value at neutral pH. The value of "n" in Eq. 8 is important to determine the mechanism of drug release. When $n < 0.45$, the Fickian diffusion process prevails, while when n value is between 0.45 and 1, it indicates anomalous transport or non-fickian transfer mechanism (Shakouri et al., 2023). The n value at neutral pH was 0.738, and at acidic pH was 0.603, both higher than 0.45, which means the drug release obeys anomalous release. It is

important to note that the value of n is lower at acidic pH than at neutral, which indicates that diffusion replaced dissolution and destruction of the polymer matrix as the primary release mechanism because higher "n" values are more likely to be associated with the dissolution mechanism (Aarabi et al., 2023). The physical and chemical interactions between 5-FU and the nanocomposite components play a pivotal role in preserving the structural integrity of the nanocarrier and preventing its dissolution under physiological conditions. Consequently, the release profile under neutral conditions is mainly based on diffusion, in agreement with the results reported earlier (Pirali et al., 2023). Additionally, the K parameter increases as the pH decreases, corroborating that the drug release rate is faster in the acidic environment.

Table 2 R^2 and other parameters obtained from different kinetic models applied to 5-FU release data from G/PEG/g-C_3N_4 nanocomposite.

pH	Zero-Order		First-Order		Higuchi		Korsmeyer-Peppas		
	k_0	R^2	K_1	R^2	k_H	R^2	k_{KP}	R^2	n
5.4	1.195	0.926	0.035	0.928	10.407	0.992	6.93	0.985	0.603
7.4	1.074	0.981	0.028	0.937	10.090	0.949	3.14	0.984	0.738

3.7. Investigation of Cytotoxicity

To investigate the cytotoxicity of G, G/PEG, G/PEG/g-C_3N_4, G/PEG/g-C_3N_4/5-FU, and free 5-FU, the MTT test was carried out on breast cancer cells (Fig.5), as detailed in the materials and methods section. The control group, which had not been treated with any material, was used to compare the cell viability of the samples. Cell viability was around 97%, 99.0%, and 93.0% when exposed to G, G/PEG, and G/PEG/g-C_3N_4, respectively, indicating that these samples exhibited no substantial cytotoxicity and were biocompatible. However, a slight reduction in cell viability was obtained after adding g-C_3N_4, though the value is still over 90%. According to ISO standards (ISO, 2009), bionanocomposites with a cell viability higher than 80% can be regarded as non-cytotoxic. Therefore, the polymers and nanoparticles used herein can be considered as non-toxic. 5-FU encapsulated in G/PEG/g-C_3N_4 dramatically reduced the cell viability, even more than free 5-FU, which confirms that the nanocarrier developed herein is more efficient than unbound 5-FU for cancer therapy. The nanocomposite releases 5-FU in a sustained manner over a period of time. However, 5-FU is an insoluble drug; hence it is likely to bypass the release mechanism and interact directly with cells via lipid membrane penetration. Overall, MTT results indicated that the use of G/PEG/g-C_3N_4/5-FU nanocomposite increased the rate of 5-FU penetration into MCF-7 cancer cells.

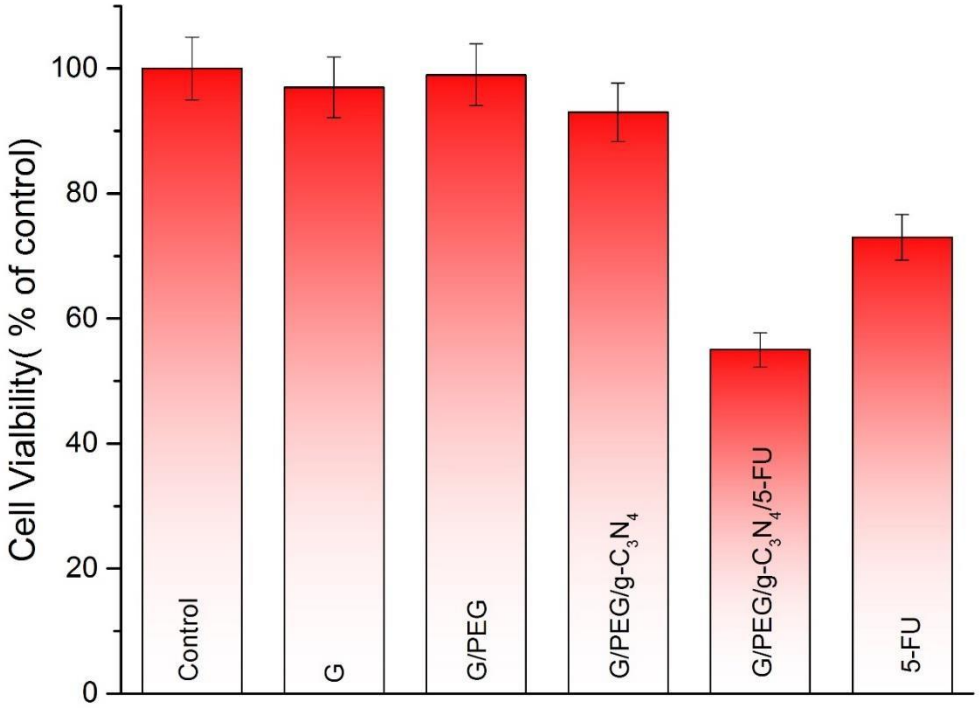

Fig.5 In vitro cytotoxic activity of G, G/PEG, G/PEG/g-C_3N_4, G/PEG/g-C_3N_4/5-FU, and free 5-FU on MCF-7 cells after 48 hours of incubation (p-value< 0.05 in comparison to the control group; Mean values ± SD, n=3 The error bars were calculated as the standard deviation divided by the square root of the number of measurements).

3.8. Cell apoptosis assay

Necrosis and apoptosis on breast cancer cells treated with G, G/PEG, G/PEG/g-C_3N_4, G/PEG/g-C_3N_4/5-FU, and free 5-FU were examined by flow cytometry (Fig.6) to learn more about the biological characteristics of the developed DDS. The flow cytometry chart is divided into four quadrants, labeled Q1 for necroptotic cells (FITC-/PI+), Q2 for cells in the late apoptotic stage (FITC+/PI+), Q3 for cells in the early apoptotic stage (FITC+/PI-), and Q4 for cells that are still alive (FITC-/PI-). The total apoptotic percentage for the control group was 8.93%, with 7.83% necrotic, indicating normal viability for these cells. The cell viability of MCF-7 cells treated with G/PEG/g-C_3N_4 nanocarrier hardly changed after 48 h of treatment compared with the control, thus corroborating the biocompatibility of the nanocarrier. Nevertheless, the cell apoptosis percentage at early-stage slightly increased (from 6.76% to 11.2%) compared to the control, pointing out the capability of g-C_3N_4 to induce apoptosis in MCF-7 cells. On the other hand, cells treated with G/PEG/g-C_3N_4/5-FU showed the lowest viability percentage, and only 17.8% of MCF-7 cells were still alive, which is the highest cell death rate among all the groups, even higher than that of free 5-FU (33.8% of MCF-7 cells were still alive after treatment with the free drug). Additionally, G/PEG/g-C_3N_4/5-FU showed lower necrotic cell percentage than unbound 5-FU, indicating that more cells were in early apoptosis or late phases than necrotic ones (Q1). The drug-loaded nanocomposite revealed much higher late apoptotic (46.7% vs. 3.04%) and early apoptotic

percentage (22.1% vs. 11.6%) than free 5-FU, demonstrating that the use of G/PEG/g-C_3N_4 as nanocarrier and the continuous drug release enhances the apoptotic activation of 5-FU. Overall, the lowest cell survival percentage (17.8%) and the highest cell percentage in the primary (22.1%) and secondary apoptosis (46.7%) stages correspond to cells treated with G/PEG/g-C_3N_4/5-FU nanocomposite. The developed DDS resulted in only 13.3 % necrosis, which is almost 4-fold lower than that of free 5-FU, indicative of a highly-programmed cell death. Therefore, flow cytometry results indicate that the loading of 5-FU into the nanocarrier enhances toxicity against cancerous cells through improved induction of apoptosis. Overall, it can be concluded that the G/PEG/g-C_3N_4/5-FU nanocomposite has acceptable toxicity and gradual release against cancer cells.

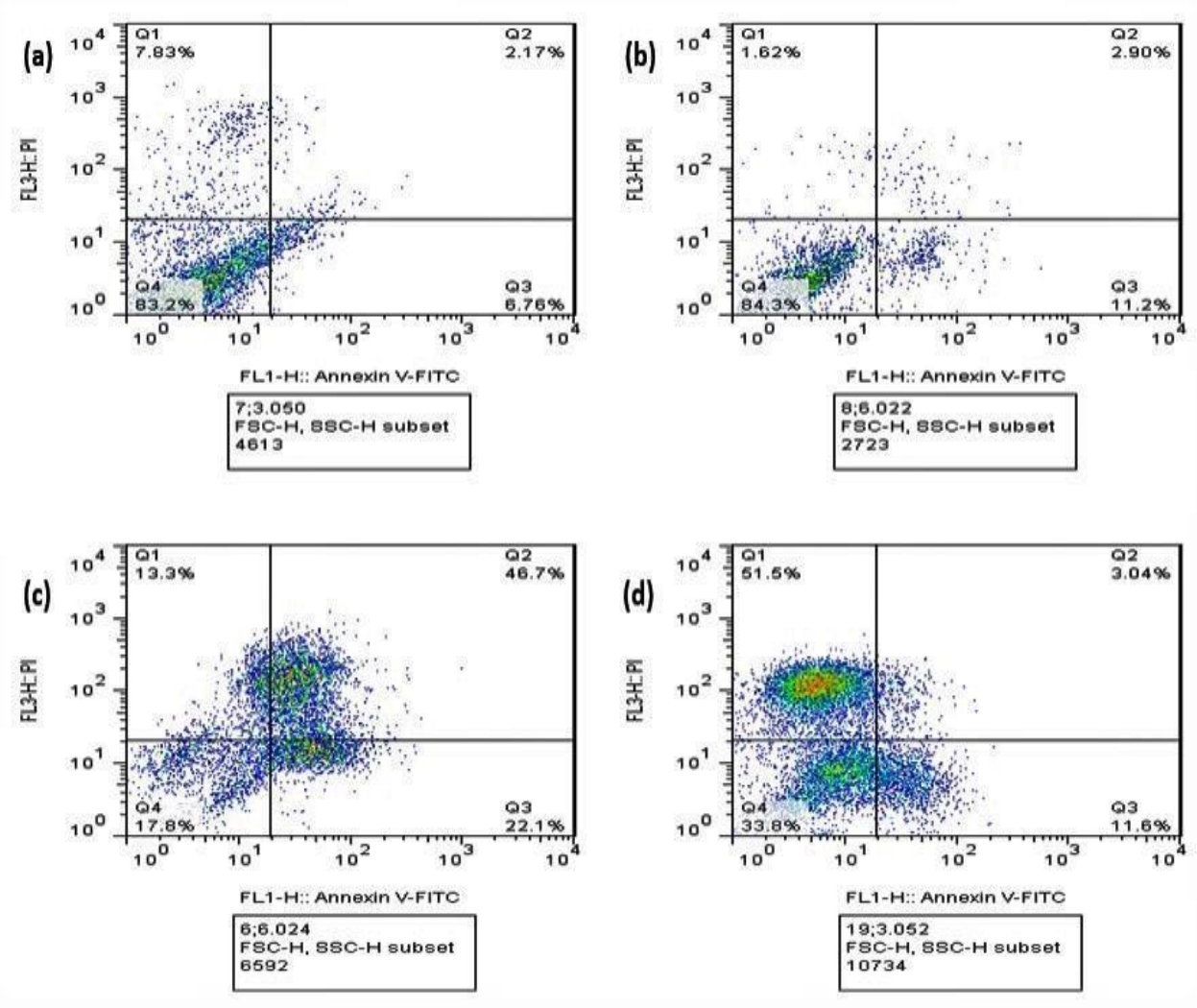

Fig.6 Flow cytometry analysis of annexin V/propidium iodide (PI) staining of MCF-7 cells treated with the control group (a) G/PEG/g-C_3N_4 (b), G/PEG/g-C_3N_4/5-FU (c), and free 5-FU (d). The bottom left quadrant (annexin V-/PI-) represents viable cells; the top left (annexin V−/PI+), necrotic cells; the bottom right (annexin V+/PI−), early apoptotic cells; and the top right (annexin V+/PI+), late apoptotic cells.

4. Conclusion

A pH-responsive nanocarrier (G/PEG/g-C_3N_4) for targeted 5-FU delivery towards breast cancer cells has been synthesized via simple and green double emulsion technique. The crystalline nature of the nanocomposite components and their interactions were investigated via FT-IR and XRD techniques. Its surface morphology was explored via FESEM, which revealed the uniformity and spherical shape of the nanocarrier. Also, the zeta potential was +35.4 mV, corroborating its high colloidal stability. The encapsulation efficiency (89%) and drug loading (47%) were significantly higher than those found for other 5-FU nanocarriers. The release study showed a gradual and controlled release of 5-FU for 96 h, and 98% of 5-FU was released from the nanocarrier at pH 5.4. Further, the drug was released faster in the acidic environment of a tumor than in normal physiological conditions. MTT assay demonstrated that the G/PEG/g-C_3N_4/5-FU nanocomposite had the lowest cell viability among the samples and a significant toxic effect on breast cancerous cells. In addition, flow cytometry confirms that using G/PEG/g-C_3N_4 as a nanocarrier can improve apoptotic activation of 5-FU, and that the drug-loaded nanocomposite showed much higher total apoptotic percentage (66.8%) than the free 5-FU (14.64%). On the other hand, the free drug exhibited a higher amount of necroptotic cells (51.5% vs 13.3%). This indicates the potential of the nanocarrier to enhance apoptosis induction and reduce the side effects of 5-FU. Overall, the DDS developed herein can be considered an effective therapeutic platform for breast cancer treatment. However, it cannot be used through the oral pathway since it is pH-sensitive and unstable in the acidic environment of the stomach. Additionally, its cytotoxicity towards other cell lines, such as L929 normal cell lines, 4T1 cell lines, etc., should be assessed. Furthermore, it can be studied as an injectable pH-sensitive nanocarrier, evaluating its therapeutic performance in terms of tumor growth and breast cancer treatment in animal models and pharmacodynamic studies. *In vivo* experiments should be performed to confirm that the developed nanocomposite is a promising candidate for cancer therapy. Future work could also focus on investigating the effectiveness of this nanocarrier for the delivery of other drugs or even two anti-cancer drugs simultaneously.

Funding: Financial support from the Community of Madrid within the framework of the multi-year agreement with the University of Alcalá in the line of action "Stimulus to Excellence for Permanent University Professors", Ref. EPU-INV/2020/012, is gratefully acknowledged

Declaration of competing interest

The authors declare no conflict of interest.

Data availability statement

The data within this article will be available upon contacting the corresponding authors.

References

Aarabi, P., Pourmadadi, M., Yazdian, F., Rashedi, H., Khoshmaram, K., Navaei, M., 2023. Synthesis and characterization of a novel , pH-responsive sustained release nanocarrier

using polyethylene glycol , graphene oxide , and natural silk fibroin protein by a green nano emulsification method . Int. J. Biol. Macromol. 226, 1100–1115. https://doi.org/10.1016/j.ijbiomac.2022.11.226

Antonio, A., Martino, D., Kucharczyk, P., Petr, C., Vladimir, H., 2017. Chitosan-based nanocomplexes for simultaneous loading, burst reduction and controlled release of doxorubicin and 5-fluorouracil. Int. J. Biol. Macromol. https://doi.org/10.1016/j.ijbiomac.2017.04.004

Azizi, M., Ghourchian, H., Yazdian, F., Alizadehzeinabad, H., 2018. Albumin coated cadmium nanoparticles as chemotherapeutic agent against MDA-MB 231 human breast cancer cell line. Artif. Cells, Nanomedicine Biotechnol. 46, 787–797. https://doi.org/10.1080/21691401.2018.1436064

Bhasarkar, J., Bal, D., 2019. Kinetic investigation of a controlled drug delivery system based on alginate scaffold with embedded voids. Journal of Applied Biomaterials & Functional Materials. https://doi.org/10.1177/2280800018817462

Boddu, A., Obireddy, S.R., Subbarao, S.M.C., Rao, K.M., Venkata, K.R.K.S., 2021. Encapsulation of 5-Fluorouracil Treated Reduced Graphene Oxide in Sodium Alginate Matrix for Controlled and pH-Responsive Drug Delivery. ChemistrySelect 6, 6533–6540. https://doi.org/10.1002/slct.202101395

Chatterjee, K., Sarkar, S., Rao, K.J., Paria, S., 2014. Core/shell nanoparticles in biomedical applications. Adv. Colloid Interface Sci. 209, 8–39. https://doi.org/10.1016/j.cis.2013.12.008

Chieng, B.W., Ibrahim, N.A., Yunus, W.M.Z.W., Hussein, M.Z., 2014. Poly(lactic acid)/poly(ethylene glycol) polymer nanocomposites: Effects of graphene nanoplatelets. Polymers (Basel). 6, 93–104. https://doi.org/10.3390/polym6010093

Curcio, M., Altimari, I., Gianfranco, U., Cirillo, G., Vittorio, O., Puoci, F., Picci, N., Iemma, F., 2013. Biodegradable gelatin-based nanospheres as pH-responsive drug delivery systems. Journal of Nanoparticle Research. https://doi.org/10.1007/s11051-013-1581-x

Deng, H., Dong, A., Song, J., Chen, X., 2019. Injectable thermosensitive hydrogel systems based on functional PEG / PCL block polymer for local drug delivery. J. Control. Release 297, 60–70. https://doi.org/10.1016/j.jconrel.2019.01.026

Dong, J., Zhao, Y., Chen, H., Liu, L., Zhang, W., Sun, B., Yang, M., Wang, Y., Dong, L., 2018. Fabrication of PEGylated graphitic carbon nitride quantum dots as traceable, pH-sensitive drug delivery systems. New J. Chem. 42, 14263–14270. https://doi.org/10.1039/c8nj02542h

Duan, F., Zhang, S., Yang, L., Zhang, Z., He, L., Wang, M., 2018. Bifunctional aptasensor based on novel two-dimensional nanocomposite of MoS_2 quantum dots and g-C_3N_4 nanosheets decorated with chitosan-stabilized Au nanoparticles for selectively detecting prostate specific antigen. Anal. Chim. Acta 1036, 121–132. https://doi.org/10.1016/j.aca.2018.06.070

Eslami, P., Davarpanah, L., Vahabzadeh, F., 2016. Encapsulating role of β-cyclodextrin in formation of pickering water-in-oil-in-water (W1/O/W2) double emulsions containing

Lactobacillus dellbrueckii. Food Hydrocoll 133-148. https://doi.org/10.1016/j.foodhyd.2016.10.035

Ethirajan, A., Schoeller, K., Musyanovych, A., Ziener, U., Landfester, K., 2008. Synthesis and optimization of gelatin nanoparticles using the miniemulsion process. Biomacromolecules 9, 2383–2389. https://doi.org/10.1021/bm800377w

Fu, C., Wu, C., Chien, C., Hsu, T., Ou, S., n.d. Polyethylene $Glycol_{6000}$/carbon Nanodots as Fluorescent Bioimaging Agents. Nanomaterials 1–15. https://doi.org/10.3390/nano10040677

Guo, Y., Chen, Y., Han, P., Liu, Y., Li, W., Zhu, F., Fu, K., Chu, M., 2019. Biocompatible Chitosan-Carbon Nanocage Hybrids for Sustained Drug Release and Highly Efficient Laser and Microwave Co-irradiation Induced Cancer Therapy. Acta Biomater. https://doi.org/10.1016/j.actbio.2019.12.010

Habibi, M., Hosseini, S., Mahboobnia, K., 2019b. Simultaneous controlled release of 5-FU , DOX and PTX from chitosan /PLA/5-FU /g-C_3N_4-DOX / g-C_3N_4-PTX triaxial nano fibers for breast cancer treatment in vitro. Colloids Surfaces B Biointerfaces 179, 495–504. https://doi.org/10.1016/j.colsurfb.2019.04.026

He, K., Xie, J., Li, M., Li, X., 2018. In situ one-pot fabrication of g-C_3N_4 nanosheets/NiS cocatalyst heterojunction with intimate interfaces for efficient visible light photocatalytic H_2 generation. Appl. Surf. Sci. 430, 208–217. https://doi.org/10.1016/j.apsusc.2017.08.191

Houshyari, A., Heydari, M., Bagheri, M., Nezafati, N., 2018. Preparation of gelatin nanoparticles by a water-in-oil emulsion method for water-soluble model drug encapsulation. Mater. Today Proc. 5, 15800–15805. https://doi.org/10.1016/j.matpr.2018.05.077

ISO 10993-5:2009 Biological Evaluation of Medical Devices. Part 5: Tests for In Vitro Cytotoxicity. International Organization for Standardization; Geneva, Switzerland: 2009

Kačuráková, M., Wilson, R.H., 2001. Developments in mid-infrared FT-IR spectroscopy of selected carbohydrates. Carbohydr. Polym. 44, 291–303. https://doi.org/10.1016/S0144-8617(00)00245-9

Khan, H., Shukla, R.N., Bajpai, A.K., 2016. Genipin-modified gelatin nanocarriers as swelling controlled drug delivery system for in vitro release of cytarabine. Mater. Sci. Eng. C 61, 457–465. https://doi.org/10.1016/j.msec.2015.12.085

Kumar, A., Kumar, P., Joshi, C., Manchanda, M., Boukherroub, R., Jain, S.L.,2016. Nickel Decorated on Phosphorous-Doped Carbon Nitride as an Efficient Photocatalyst for Reduction of Nitrobenzenes. Nanomaterials.. https://doi.org/10.3390/nano6040059

Lee, J.J., Beumer, J.H., Chu, E., 2016. Therapeutic drug monitoring of 5-fluorouracil. Cancer Chemother. Pharmacol. 78, 447–464. https://doi.org/10.1007/s00280-016-3054-2

Lin, L., Cong, Z., Li, J., Ke, K., Guo, S., Yang, H., Chen, G., 2014. photosensitizers and pH-responsive drug nanocarriers for cancer imaging and therapy. J. Mater. Chem. B, 1031–1037. https://doi.org/10.1039/c3tb21479f

Liu, S., Ye, T., Liu, Y., Cheng, H., Liu, X., 2020. Graphitic‐carbon nitride nanosheets as a new

inorganic filler for improving energy storage density of PVDF - based dielectric composites. J. Mater. Sci. Mater. Electron. 31, 13063–13069. https://doi.org/10.1007/s10854-020-03856-z

Mahmud, M., Rahman, A.F.M.M., Salem, K.S., Bari, L., 2022. Architecting Ultrathin Graphitic C_3N_4 Nanosheets Incorporated PVA/Gelatin Bionanocomposite for Potential Biomedical Application : Effect on Drug Delivery, Release Kinetics, and Antibacterial Activity. ACS Appl. Bio Mater. https://doi.org/10.1021/acsabm.2c00502

Malekimusavi, H., Ghaemi, A., Masoudi, G., Chogan, F., Rashedi, H., Javadi, S., Haghiralsadat, B.F., Teimouri, M., Hamedani, N.F., 2019. Graphene oxide-L-arginine nanogel : A pH-sensitive fluorouracil nanocarrier. Biotechnology and Applied Biochemistry1–9. https://doi.org/10.1002/bab.1768

Mano, J.F., Koniarova, D., Reis, R.L., 2003. Thermal properties of thermoplastic starch/synthetic polymer blends with potential biomedical applicability. J. Mater. Sci. Mater. Med. 14, 127–135. https://doi.org/10.1023/A:1022015712170

Martha, S., Nashim, A., Parida, K.M., 2013. Facile synthesis of highly active g-C_3N_4 for efficient hydrogen production under visible light. J. Mater. Chem. A 1, 7816–7824. https://doi.org/10.1039/c3ta10851a

Mckenzie, M., Betts, D., Suh, A., Bui, K., Kim, L.D., 2015. Hydrogel-Based Drug Delivery Systems for Poorly Water-Soluble Drugs. Molecules 20397–20408. https://doi.org/10.3390/molecules201119705

Miralinaghi, P., Kashani, P., Moniri, E., Miralinaghi, M., 2019. Non-linear kinetic, equilibrium, and thermodynamic studies of 5- fluorouracil adsorption onto chitosan – functionalized graphene oxide Non-linear kinetic , equilibrium , and thermodynamic studies of 5-fluorouracil adsorption onto chitosan – functional.https://doi.org/ 10.1088/2053-1591/ab0831

Mohebali, A., 2021. Fabrication and characterization of pH-responsive poly (methacrylic acid) -based molecularly imprinted polymers nanosphere for controlled release of amitriptyline hydrochloride Fabrication of MIP for amitriptyline hydrochloride. Polymers for Advanced Technologies 1–11. https://doi.org/10.1002/pat.5440

Xiaodong Zhang, Xiao Xie, Hui Wang, Jiajia Zhang, Bicai Pan, and Yi Xie., 2013. Enhanced Photoresponsive Ultrathin Graphitic-Phase C_3N_4 Nanosheets for Bioimaging. J. Am. Chem. Soc.18–21. https://doi.org/10.1021/ja308249k

Niu, P., Zhang, L., Liu, G., Cheng, H.M., 2012. Graphene-like carbon nitride nanosheets for improved photocatalytic activities. Adv. Funct. Mater. 22, 4763–4770. https://doi.org/10.1002/adfm.201200922

Norouzi, M., Nazari, B., Miller, D.W., 2016. Injectable hydrogel-based drug delivery systems for local cancer therapy. Drug Discov. Today. https://doi.org/10.1016/j.drudis.2016.07.006

Pirali, A., Pourmadadi, M., Yazdian, F., Rashedi, H., Rahdar, A., Díez-pascual, A.M., 2023. Journal of Drug Delivery Science and Technology. pH-sensitive ameliorated quercetin delivery using graphene oxide nanocarriers coated with potential anticancer gelatin-

polyvinylpyrrolidone nanoemulsion with bitter almond oil. J. Drug Deliv. Sci. Technol. 82, 104339. https://doi.org/10.1016/j.jddst.2023.104339

Pourmadadi, M., Darvishan, S., Abdouss, M., Yazdian, F., Rahdar, A., Díez-Pascual, A.M., 2023a. pH-responsive polyacrylic acid (PAA)-carboxymethyl cellulose (CMC) hydrogel incorporating halloysite nanotubes (HNT) for controlled curcumin delivery. Ind. Crops Prod. 197, 116654. https://doi.org/10.1016/j.indcrop.2023.116654

Pourmadadi, M., Ahmadi, M., Yazdian, F., 2023b. Synthesis of a novel pH-responsive Fe_3O_4 /chitosan/agarose double nanoemulsion as a promising Nanocarrier with sustained release of curcumin to treat MCF-7 cell line. Int. J. Biol. Macromol. 235, 123786. https://doi.org/10.1016/j.ijbiomac.2023.123786

Prabha, G., Raj, V., 2016. Preparation and characterization of chitosan - Polyethylene glycol-polyvinylpyrrolidone-coated superparamagnetic iron oxide nanoparticles as carrier system: Drug loading and in vitro drug release study. J. Biomed. Mater. Res. - Part B Appl. Biomater. 104, 808–816. https://doi.org/10.1002/jbm.b.33637

Qi, K., Zada, A., Yang, Y., Chen, Q., Khataee, A., 2020. Design of 2D–2D NiO/g-C_3N_4 heterojunction photocatalysts for degradation of an emerging pollutant. Res. Chem. Intermed. 46, 5281–5295. https://doi.org/10.1007/s11164-020-04262-0

Radev, L., Fernandes, M.H. V., Salvado, I.M., Kovacheva, D., 2009. Organic/inorganic bioactive materials part III: In vitro bioactivity of gelatin/silicocarnotite hybrids. Cent. Eur. J. Chem. 7, 721–730. https://doi.org/10.2478/s11532-009-0078-z

Raziq, F., Sun, L., Wang, Y., Zhang, X., Humayun, M., 2017. Synthesis of Large Surface-Area g-C_3N_4 Comodified with MnO_x and Au-TiO_2 as Efficient Visible-Light Photocatalysts for Fuel Production. Advanced Energy Materials 1701580, 2–11. https://doi.org/10.1002/aenm.201701580

Requena, J., Brooks, D.E., Haydon, D.A., 1977. van der Waals Forces in Oil/Water Systems. Plenary Invit. Lect. 58, 27–36. https://doi.org/10.1016/b978-0-12-404501-9.50011-0

Ribeiro, S.B., Araújo, A.A. de, Oliveira, M.M.B., Silva, A.M. dos S., Silva-Júnior, A.A. da, Guerra, G.C.B., Brito, G.A. de C., Leitão, R.F. de C., Júnior, R.F. de A., Garcia, V.B., Vasconcelos, R.C., deMedeiros, C.A.C.X., 2021. Effect of dexamethasone-loaded PLGA nanoparticles on oral mucositis induced by 5-fluorouracil. Pharmaceutics 13, 1–18. https://doi.org/10.3390/pharmaceutics13010053

Sang, Y., Miao, P., Chen, T., Zhao, Y., Chen, L., Tian, Y., Han, X., Gao, J., 2022. Fabrication and Evaluation of Graphene Oxide/Hydroxypropyl Cellulose/Chitosan Hybrid Aerogel for 5-Fluorouracil Release. Gels 8. https://doi.org/10.3390/gels8100649

Schöttler, S., Becker, G., Winzen, S., Steinbach, T., Mohr, K., Landfester, K., Mailänder, V., Wurm, F.R., 2016. Protein adsorption is required for stealth effect of poly(ethylene glycol)- and poly(phosphoester)-coated nanocarriers. Nat. Nanotechnol. 11, 372–377. https://doi.org/10.1038/nnano.2015.330

Shakouri, S., Pourmadadi, M., Abdouss, M., Rahdar, A., 2023. pH-responsive double emulsion system for targeted anticancer therapy based on polyacrylic acid-polyvinyl pyrrolidone

containing carbon nanotubes for 5-fluorouracil as an anticancer medication. Inorg. Chem.
Commun. 158, 111494. https://doi.org/10.1016/j.inoche.2023.111494

Shameli, K., Ahmad, M. Bin, Jazayeri, S.D., Sedaghat, S., Shabanzadeh, P., Jahangirian, H., Mahdavi, M., Abdollahi, Y., 2012. Synthesis and characterization of polyethylene glycol mediated silver nanoparticles by the green method. Int. J. Mol. Sci. 13, 6639–6650. https://doi.org/10.3390/ijms13066639

Sun, W., Chen, Y., Yuan, W., 2013. Hemostatic absorbable gelatin sponge loaded with 5-fluorouracil for treatment of tumors. Int. J. Nanomedicine 8, 1499–1506. https://doi.org/10.2147/IJN.S41462

Sweah, Z.J., Al-Lami, H.S., Haddad, A.M., 2016. Preparation and Swelling Behavior of L-Lactide Interpenetrating Networks. Open J. Org. Polym. Mater. 06, 119–133. https://doi.org/10.4236/ojopm.2016.64012

Wang, F., Li, J., Tang, X., Huang, K., Chen, L., 2020. Polyelectrolyte three layer nanoparticles
of chitosan/dextran sulfate/chitosan for dual drug delivery. Colloids Surfaces B Biointerfaces 190, 110925. https://doi.org/10.1016/j.colsurfb.2020.110925

Wen, J., Xie, J., Chen, X., Li, X., 2017. A review on g-C_3N_4-based photocatalysts. Appl. Surf. Sci. 391, 72–123. https://doi.org/10.1016/j.apsusc.2016.07.030

Yi, C., Xu, Q., Yang, D., Wang, M., 2022. A novel pH-responsive charge reversal nanospheres
based on acetylated histidine-modified lignin for drug delivery. Ind. Crop. Prod. 186, 115193. https://doi.org/10.1016/j.indcrop.2022.115193

Yi, H., Cho, H.J., Cho, S.M., Lee, D.G., Abd El-Aty, A.M., Yoon, S.J., Bae, G.W., Nho, K., Kim, B., Lee, C.H., Kim, J.S., Bartlett, M.G., Shin, H.C., 2010. Pharmacokinetic properties
and antitumor efficacy of the 5-fluorouracil loaded PEG-hydrogel. BMC Cancer 10. https://doi.org/10.1186/1471-2407-10-211

Zhang, W.J., Yan, Y.Z., Nagappan, S., He, S., Ha, C.S., Jin, Y.S., 2021. Dual (thermo-/pH-) responsive P(NIPAM-co-AA-co-HEMA) nanocapsules for controlled release of 5-fluorouracil. J. Macromol. Sci. Part A Pure Appl. Chem. 58, 860–871. https://doi.org/10.1080/10601325.2021.1964368

Zhao, L., Liu, J., Zhang, L., Gao, Y., Zhang, Z., Luan, Y., 2013. Self-assembly properties , aggregation behavior and prospective application for sustained drug delivery of a drug-participating catanionic system. Int. J. Pharm. 452, 108–115. https://doi.org/10.1016/j.ijpharm.2013.04.072

Zhu, M., Wang, Y., Wang, F., Li, L., Qiu, X., 2021. CircFBXL5 promotes the 5-FU resistance of breast cancer via modulating miR-216b/HMGA2 axis. Cancer Cell Int. 21, 1–12. https://doi.org/10.1186/s12935-021-02088-3